PCCP

PAPER

Enhanced hydrogen sensing properties of graphene by introducing a mono-atom-vacancy

Q. G. Jiang,[ab] Z. M. Ao,*[bc] W. T. Zheng,[a] S. Li[b] and Q. Jiang*[a]

To facilitate the dissociative adsorption of H_2 molecules on pristine graphene, the addition of a mono-atom-vacancy to graphene is proposed. This leads to reduction of the dissociative energy barrier for a H_2 molecule on graphene from 3.097 to 0.805 eV for the first H_2 and 0.869 eV for the second, according to first principles calculations. As a result, two H_2 molecules can be easily dissociatively adsorbed on this defected graphene at room temperature. The electronic structure and conductivity of the graphene change significantly after H_2 adsorption. In addition, the related dissociative adsorption phase diagrams under different temperatures and partial pressures show that this dissociative adsorption at room temperature is very sensitive (10^{-35} mol L^{-1}). Therefore, this defected graphene is promising for ultra-sensitive room temperature hydrogen sensing.

1. Introduction

Hydrogen has attracted great interest because it is a clean and renewable energy source.[1] Hydrogen is widely present in nuclear reactors, coal mines and semiconductor manufacturing, *etc.*[2] Because hydrogen is highly flammable and explosive with a volume concentration of more than 4%, developing highly sensitive hydrogen sensors is important. Commercially, hydrogen sensors are mainly composed of metal oxide (*e.g.*, SnO_2) films based on the chemresistive mechanism.[3–7] However, to obtain satisfactory results by using metal oxide sensors a temperature over 400 °C is usually required,[8] which is energy intensive and may trigger an explosion. Therefore, it is desirable to develop new types of hydrogen sensors which operate at room temperature.

Although graphene has definite advantages over other gas sensing materials,[9] due to its excellent electronic[10] and mechanical properties,[11] the interaction between pristine graphene and H_2 molecules is weak due to the inert nature of graphene.[12] It is known that when graphene is synthesized using chemical techniques, such as chemical vapor deposition (CVD)[13] and aqueous dispersion methods,[14] vacancies could be present. Vacancies can also be introduced into graphene using the ion irradiation technique.[15,16] These vacancies can promote the reactivity of graphene and facilitate the dissociative adsorption of small molecules on graphene.[17–19] Thus, we expect that H_2 molecules could be dissociatively adsorbed on vacancies in the graphene and this adsorption may change the electronic properties of the graphene.

In this paper, we will consider the dissociative adsorption of H_2 molecules on graphene with mono-atom-vacancies by using density functional theory (DFT) calculations. It is found that the defected graphene results in an evident drop of the dissociative energy barrier of H_2. This adsorption evidently influences the conductivity of the defected graphene. In addition, the phase diagram of H_2 dissociative adsorption on graphene under different temperatures and partial pressures is established based on DFT results and thermodynamic parameters, which confirm the sensitivity of hydrogen dissociative adsorption and the sensitivity of the graphene for hydrogen detection.

2. Calculation methods and thermodynamic model

All calculations are implemented by Dmol³ code.[20] The generalized gradient approximation (GGA) with a Perdew–Burke–Ernzerhof (PBE) functional is employed to describe the exchange and correlation effects.[21] Double numerical plus polarization (DNP) is employed as the basis set. A convergence tolerance of energy of 10^{-5} Hartree is taken (1 Hartree = 27.21 eV), and the maximal allowed force and displacement are 0.002 Hartree $Å^{-1}$ and 0.005 Å, respectively. It was reported that the selection of the exchange–correlation functional has an evident effect on the resulting adsorption energies. However, the effect on the

[a] *Key Laboratory of Automobile Materials (Jilin University), Ministry of Education, and School of Materials Science and Engineering, Jilin University, Changchun 130022, China. E-mail: jiangq@jlu.edu.cn*

[b] *School of Materials Science and Engineering, The University of New South Wales, Sydney, NSW 2052, Australia. E-mail: zhimin.ao@uts.edu.au*

[c] *Centre for Clean Energy Technology, School of Chemistry and Forensic Science, Faculty of Science, University of Technology, Sydney, PO Box 123, Broadway, Sydney, NSW 2007, Australia*

calculated energy barriers is much smaller.[22] To investigate the minimum energy pathway for dissociative adsorption of a H_2 molecule on graphene, the linear synchronous transit/quadratic synchronous transit (LST/QST)[23] and nudged elastic band (NEB)[24] tools in the Dmol[3] module are used, which have been well validated for determining the structure of the transition state and the minimum energy pathway. In the simulation, three-dimensional periodic boundary conditions are taken. The simulation cell consists of a 4×4 graphene supercell with a vacuum width of 20 Å above the graphene layer to minimize the interlayer interaction. The k-point is set to $5 \times 5 \times 1$ and all atoms are allowed to relax. The DFT+D method within the Grimme scheme[25] is used in all calculations to consider the van der Waals forces.

For a H_2 molecule adsorbed on graphene before and after the dissociative adsorption, the adsorption energy E_{ad} is determined by,

$$E_{ad} = E_{H_2/graphene} - (E_{graphene} + E_{H_2}) \qquad (1)$$

where $E_{H_2/graphene}$, $E_{graphene}$ and E_{H_2} are the total energies of the H_2/graphene system, the isolated graphene and a H_2 molecule in the supercell with the same lattice of graphene, respectively.

In actual applications, the temperature (T) and pressure (P) should be considered. Therefore, the Gibbs free energy $G(T,P)$ of the system was calculated as a function of T and P. The change in Gibbs free energy for the dissociative adsorption of a H_2 molecule on graphene is taken as,

$$\Delta G(T,P) = G_{H_2/graphene}(T,P) - G_{graphene}(T,P) - G_{H_2}(T,P) \qquad (2)$$

The determined DFT total energy E is related to the volume V of the unit cell at 0 K, corresponding to the Helmholtz free energy at 0 K without zero-point vibrations. Therefore, the Gibbs free energy $G(T,P)$ in eqn (2) can be determined by,[26]

$$G(T,P) = E + F^{vib}(T) + PV \qquad (3)$$

where $F^{vib}(T)$ denotes the vibrational free energy. Because $G(T,P)$ of solid phases changes little with P, the PV term in eqn (3) is neglected.[26] Thus, $G_{graphene}(T,P) = E_{graphene} + F^{vib}_{graphene}(T)$ and $G_{H_2/graphene}(T,P) = E_{H_2/graphene} + F^{vib}_{H_2/graphene}(T)$. $F^{vib}(T)$ within the harmonic approximation for n fundamental modes (with a frequency of ω_i) of the system is expressed as,[27]

$$F^{vib}(T) = \sum_{i=1}^{n} F^{vib}(T, \omega_i)$$
$$= \sum_{i=1}^{n} \frac{1}{2}\hbar\omega_i + K_B T \ln\left[1 - \exp\left(\frac{-\hbar\omega_i}{K_B T}\right)\right]. \qquad (4)$$

$F^{vib}(T)$ is thus determined by phonon calculations with CASTEP code,[28] where the norm-conserving pseudopotentials, the GGA-PBE functional, an energy cutoff of 340 eV and $5 \times 5 \times 1$ k-point meshes are used.

The Gibbs free energy of the gas phase will be strongly affected by T and P, and can be taken as,[29]

$$G_{H_2}(T,P) = E_{H_2} + \Delta H_{H_2}(T,P^0) - T\Delta S_{H_2}$$
$$+ K_B T \ln(P/P^0) + F^{vib}_{H_2}(T) \qquad (5)$$

where the first term is the DFT result, the second and third terms are the contribution of H_2 enthalpy and entropy under atmospheric pressure ($P^0 = 1$ atm), respectively, which can be obtained from a thermodynamic database.[30] The fourth term is a pressure dependent contribution (where K_B is the Boltzmann constant). In total, $\Delta G(T,P)$ in eqn (2) is further expressed as,

$$\Delta G(T,P) = E_{H_2/graphene} + F^{vib}_{H_2/graphene}(T) - E_{graphene}$$
$$- F^{vib}_{graphene}(T) - E_{H_2} - \Delta H_{H_2}(T,P^0) \qquad (6)$$
$$+ T\Delta S_{H_2} - K_B T \ln(P/P^0) - F^{vib}_{H_2}(T)$$

3. Results and discussion

We firstly consider the geometric structures of the pristine graphene and graphene with a mono-atom-vacancy as shown in Fig. 1, the corresponding vacancy concentration is 1/32. Three sp^2 dangling bonds (σ bonds) are present near the vacancy and point towards the center of the vacancy. In addition, one delocalized π dangling bond is perpendicular to the graphene surface. The vacancy undergoes a Jahn–Teller distortion upon relaxation (see Fig. 1b), where two of the nearest C atoms to the vacancy site form a weak covalent bond with bond length 2.129 Å, consistent with the reported value of 2.1 Å.[17] This distortion results in a pentagon-like structure, with the atom displaced 0.20 Å out of the surface plane, which corresponds to the literature datum of 0.18 Å.[17] The ground state of the vacancy has a magnetic moment of 1.006 μ_B (see Fig. 1b), which is consistent with the reported value of 1.04 μ_B and experimental observation.[17,31] To further understand the electronic structure of the defective graphene, the partial density of states (PDOS) of the C_1 and C_2 atoms are analyzed and shown in Fig. 1c and d, respectively.
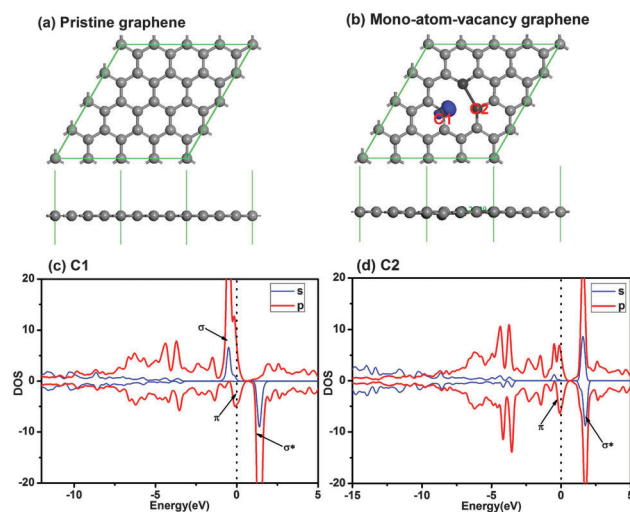
Fig. 1 The favorable configurations of pristine graphene (a), and graphene with a mono-atom-vacancy (b). The spin density of the vacancy is also shown in blue. C_1 and C_2 represent different carbon positions. The grey and black atoms are saturated and unsaturated C, respectively. The PDOS of the C_1 and C_2 atoms are shown in (c) and (d), respectively. The blue and red curves are the PDOS of the s orbital and p orbitals of the C atoms, respectively.

This journal is © the Owner Societies 2013

*Phys. Chem. Chem. Phys.*, 2013, **15**, 21016–21022 | **21017**

The spin state here is mainly contributed by the half filled σ orbital of the C_1 atom (see Fig. 1c). The C_2 atom forms a weak bond with the neighboring C atom and builds a fully empty σ^* anti-bond (see Fig. 1d) without the spin state. The half filled π bond is responsible for the p-type doping, but not for the spin state of the graphene. Therefore, formation of the pentagon saturates two of three sp^2 bonds, but the remaining unsaturated σ bond of the C_1 atom is reactive and is believed to induce the dissociative adsorption of small molecules.

For the molecular adsorption of a H_2 molecule on pristine graphene, based on the DFT+D calculations and eqn (1), the favorable adsorption site of the H_2 molecule is at the hollow site with the H–H bond parallel to the graphene surface, which is consistent with ref. 12 and shown as the initial structure, IS, in the inset of Fig. 2a. Note that it has been reported that the DFT+D method tends to over-emphasize the pair-wise inter-action energy between atoms and gives the wrong binding site for Ag atoms on graphite.[32,33] To check the correctness of our result, the literature results using vdW-DF and vdW-WF methods are compared,[34] which give the same favorable adsorption position for the H_2 molecule on graphene as our study. For the H_2 dissociative adsorption on graphene, the most favorable configuration is with two H atoms chemisorbed on the two face-to-face C atoms in the six-member ring, as shown as the final structure, FS, in Fig. 2a. LST/QST and NEB calculations indicate that this reaction is endothermic with a high energy

barrier, E_{bar}, of 3.097 eV (the energy difference between the transition state, TS, and the initial structure, IS), which is a little smaller than the reported result of 3.3 eV.[12] Therefore, the dissociative adsorption of H_2 on pristine graphene is difficult to achieve.

The obtained adsorption energy E_{ad_IS}, based on eqn (1), for graphene with a mono-atom-vacancy is listed in Table 1. The preferred structure of a H_2 molecule when adsorbed in this system is shown in Fig. 2b, which is taken as the IS in the subsequent transition state search calculations which use two possible configurations for final structures, namely with the two H atoms on the same side (named as FS_1) or on both sides (named as FS_2). In light of our DFT calculations, the FS_1 structure with a slightly higher energy of 0.2 eV is less stable than the FS_2 structure. Previous studies indicate that the H atom introduced by proton irradiation will saturate a C dangling bond and produce the FS_2 structure.[17] However, our case shows that the reaction from the IS to FS_2 is absent due to the difficulty of the H atom going through the vacancy to the other side of the graphene. Thus, only the reaction from the IS to FS_1 is discussed in the following.

After LST/QST and NEB calculations, the detailed reaction pathway and the energy barrier for the dissociative adsorption of a H_2 molecule on graphene with a mono-atom-vacancy are shown in Fig. 2b. Besides the initial and final structures, the atomic structure of the TS is also shown in Fig. 2b. It is found
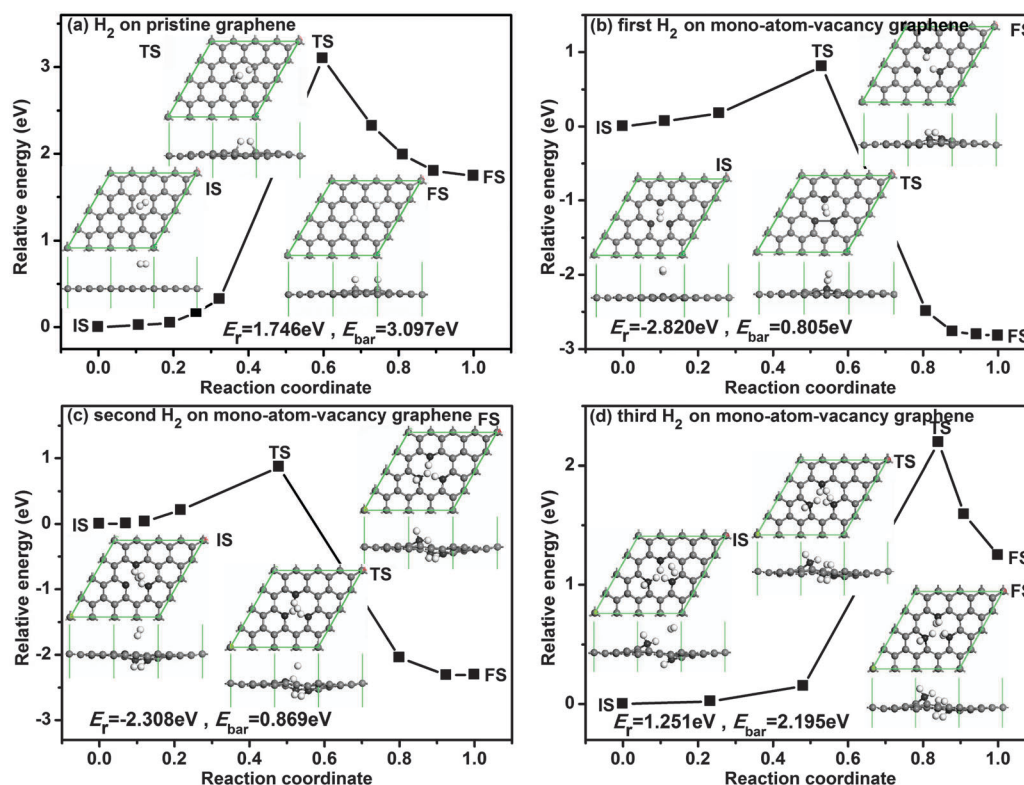
Fig. 2 The reaction pathway of H_2 molecule dissociative adsorption on pristine graphene (a), and on graphene with a mono-atom-vacancy for the first H_2 molecule (b), the second H_2 molecule (c) and the third H_2 molecule (d). IS, TS and FS represent initial structure, transition structure and final structure, respectively. Their atomic structures are shown in the inserts. The energy of the IS is taken to be zero. The units of E_{bar} and E_r are eV, where E_{bar} is the energy barrier and E_r is the reaction energy. The grey, black and white atoms are saturated C, unsaturated C and H, respectively.

21018 | *Phys. Chem. Chem. Phys.*, 2013, **15**, 21016–21022

This journal is © the Owner Societies 2013

Table 1 The adsorption energy of hydrogen in the initial structure (E_{ad_IS}) and final structure (E_{ad_FS}), the distance of the H atom above the graphene D, the H–H bond length $L_{H–H}$, and the Mulliken atomic charge of H_2 adsorption on graphene Q_{H_2}

|	E_{ad_IS} (eV)	D (Å)	$L_{H–H}$ (Å)	Q_{H_2} (e)	E_{ad_FS} (eV)
1st H_2 on pristine	−0.124	2.832	0.752	0.000	1.622
1st H_2 on mono-atom-vacancy	−0.107	2.791	0.751	−0.002	−2.927
2nd H_2 on mono-atom-vacancy	−0.159	2.169	0.755	−0.012	−2.417
3rd H_2 on mono-atom-vacancy	−0.147	2.309	0.752	0.009	1.011

that the energy barrier decreases significantly on the defective graphene, E_{bar} decreases from 3.097 eV in the pristine graphene system to 0.805 eV. The dissociative energy barrier for the first H_2 molecule on the defective graphene is slightly smaller than the reported result of 1.1 eV,[18] probably due to the different cluster graphite models and the mixed quantum mechanics/molecular mechanics methods used in the literature and in this work. In addition, the reaction also changes from being endothermic to exothermic with a negative reaction energy E_r of −2.820 eV. Since a surface reaction at ambient temperature may occur when the critical barrier of E_{cbar} is smaller than 0.91 eV,[35] this dissociative adsorption should spontaneously occur at room temperature.
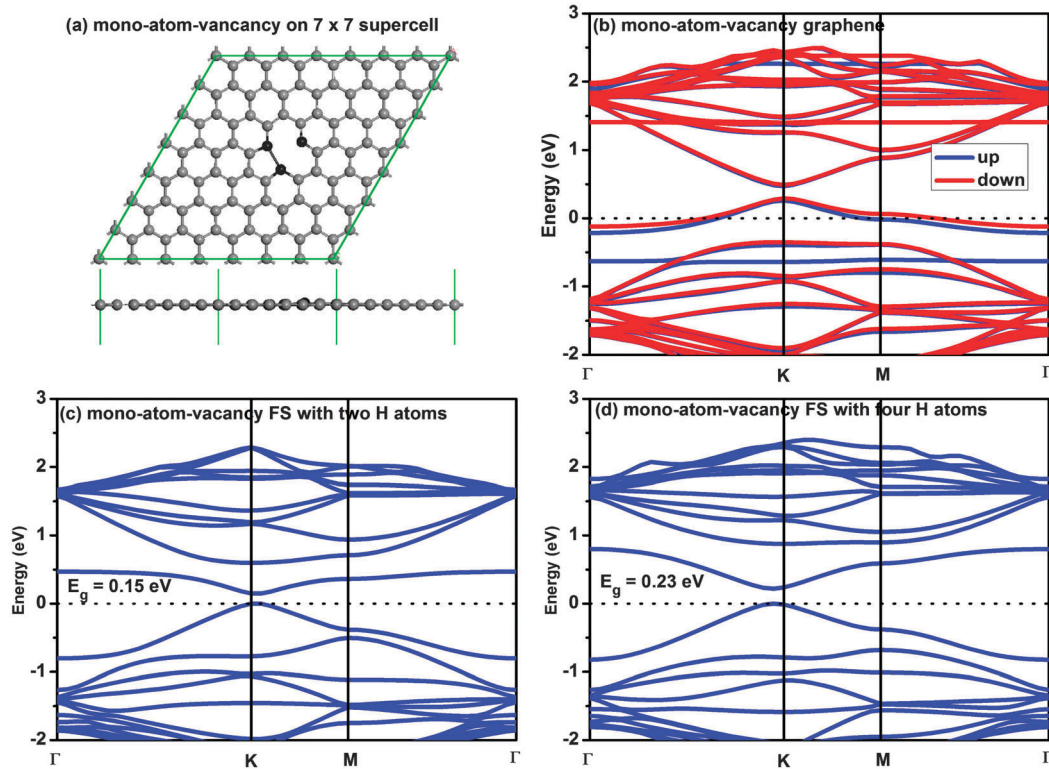
After the dissociative adsorption of the first H_2 molecule, two σ dangling bonds are saturated with H atoms, while one remaining dangling bond is still active, which may induce the adsorption of the second H_2 molecule. For the second H_2, it prefers to adsorb on the other side of the graphene opposite to the first H_2. The preferred configuration with E_{ad_IS} = 0.159 eV is shown as the IS in Fig. 2c where both dissociated H atoms

adsorb on the same C atom with the dangling bond as the most stable configuration, which is taken as the FS. Note that after the second H_2 adsorption, the first two H atoms and the two C atoms that bind with the first two H atoms, are pushed further out of the graphene layer. LST/QST and NEB calculations give E_{bar} = 0.869 eV, and E_r = −2.308 eV. Therefore, the dissociative adsorption for the second H_2 molecule can also occur smoothly at room temperature. Further dissociative adsorption of a third H_2 leads not only to a larger E_{bar} = 2.195 eV > E_{cbar} = 0.91 eV,[35] but also to a positive E_r = 1.251 eV > 0 (see Fig. 2d). As a result, the reaction can not proceed at room temperature. It is noteworthy that if we increase the size of the vacancy to two C atoms, E_{bar} = 2.166 eV for one H_2 molecule dissociative adsorption is found, indicating that this dissociative adsorption is highly unlikely at room temperature. Therefore, only the graphene system with a mono-atom-vacancy is valid for hydrogenation.

The band structure of graphene with a mono-atom-vacancy is shown in Fig. 3b, while Fig. 3a shows that of pristine graphene for comparison purposes. As expected, the bands close at the K point with the zero band gap for pristine graphene. For graphene with a
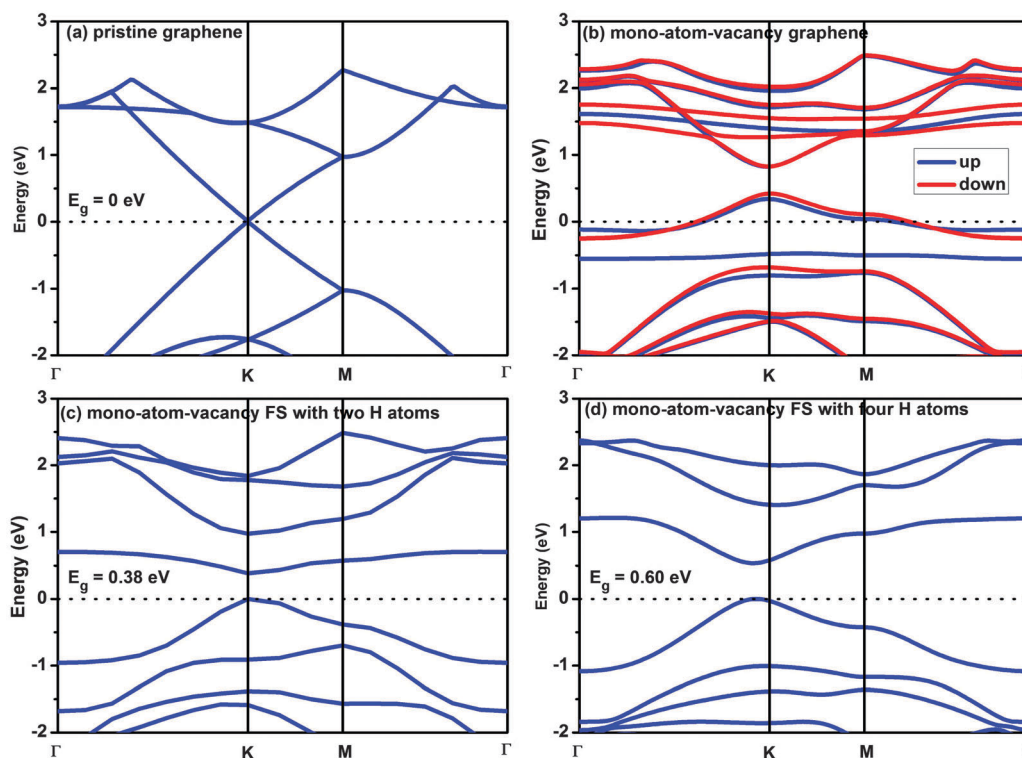
Fig. 3 The band structures of pristine graphene (a), graphene with a mono-atom-vacancy (b), the mono-atom-vacancy FS after the first dissociative adsorption of H_2 (c), and the mono-atom-vacancy FS after the second dissociative adsorption H_2 (d) in a 4 × 4 supercell. The dotted line denotes the Fermi level.
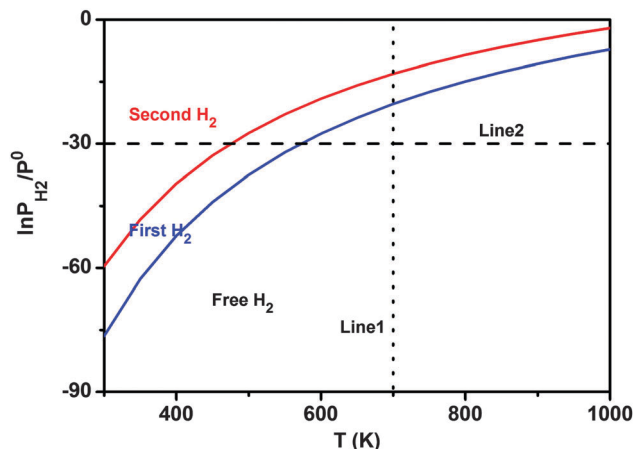
Fig. 4 The favorable configurations of graphene with a mono-atom-vacancy in a 7 × 7 supercell (a). The band structures of graphene with a mono-atom-vacancy (b), the mono-atom-vacancy FS after the first H_2 dissociative adsorption (c), and the mono-atom-vacancy FS after the second H_2 dissociative adsorption (d).

mono-atom-vacancy, the Fermi level goes down to the valence band due to the electron deficiency, indicating p-type doping. From Fig. 3c and d, we can see that the band across the Fermi level is mainly contributed by the half filled π bond, while the half filled σ bond is responsible for the spin state. The π bond has highly mobility due to the its delocalized nature, which implies that the hole mobility should be large and the graphene with a mono-atom-vacancy should be conductive. When the first H_2 is dissociated into two H atoms and adsorbed on the same side of the graphene as the mono-atom-vacancy (see Fig. 3c), the Fermi level moves up to meet the top of the valence band exactly and the graphene changes into a pristine semiconductor with band gap of 0.38 eV. Therefore, the adsorption of two H atoms degrades the conductivity of the graphene. After dissociative adsorption of the second H_2 (see Fig. 3d), the band gap increases slightly to 0.60 eV and the graphene is still a pristine semiconductor. This indicates that the change in conductivity should be small and it may be difficult to detect the dissociative adsorption of the second H_2. Thus, the detection of H_2 molecules mainly depends on the dissociative adsorption of the first H_2 molecule. Therefore, the dissociative adsorption of H_2 molecules near the vacancy can eliminate the spin state and induce a significant conductivity change, which is desirable for applications in hydrogen sensors. Although the dissociative adsorption of the second and the third H_2 molecules are studied in order to comprehensively understand the reaction between the H_2 molecule and the defective graphene, these dissociative adsorptions have little effect on the conductivity.

In reality, graphene may have a smaller vacancy concentration locally due to its disorder distribution. In order to investigate the effect of vacancy concentration on the electronic properties of graphene before and after H_2 dissociative adsorption, we further investigated the electronic structure in 7 × 7 supercell with a smaller vacancy concentration of 1/98 as shown in Fig. 4a. Fig. 4b–d show the band structures of graphene, graphene after the first H_2 dissociative adsorption, and graphene after the second H_2 dissociative adsorption, respectively. Similar changes in the electronic properties are found in this graphene system where the vacancy concentration is low. Thus, the dissociative adsorption of H_2 near a vacancy can still change the graphene from p-type doping to a pristine semiconductor, which indicates that H_2 molecules can still be detected even when the defect concentration is decreased.

To determine the sensitivity of graphene with a mono-atom-vacancy for H_2 gas detection, we proposed a phase diagram to determine the effects of T and P on the dissociative adsorption of hydrogen on graphene, which is calculated in light of eqn 6 and is shown in Fig. 5. It is known that the reaction occurs when $\Delta G(T,P) < 0$. The figure shows that at a high T or a low P, free H_2 molecules cannot dissociatively adsorb on the mono-atom-vacancy graphene. At room temperature, the first H_2 molecule starts to dissociate on the graphene at a very low partial pressure ratio $\ln P_{H_2}/P^0$ of 10^{-76}, or 10^{-35} mol L^{-1}. When partial pressure ratio $\ln P_{H_2}/P^0 > 10^{-59}$, i.e. 10^{-27} mol L^{-1}, the second H_2 molecule begins to dissociate and is adsorbed on graphene. To better understand the effects of T and P on the

21020 | *Phys. Chem. Chem. Phys.*, 2013, **15**, 21016–21022

This journal is © the Owner Societies 2013

Fig. 5 The phase diagram under different temperatures T and partial pressures P/P_0 for the first dissociative adsorption of a H_2 molecule on mono-atom-vacancy graphene (a), and that for the second H_2 molecule (b). Vertical line 1 denotes $T = 700$ K, and Horizontal line 2 denotes $\ln P/P_0 = -30$.

dissociative adsorption of H_2 on mono-vacancy graphene, lines 1 and 2 are plotted in the figure. Line 1 shows that increasing P at constant T promotes dissociative adsorption. Under a certain P as shown by line 2, low T induces dissociative adsorption. It is reported that the frequently used SnO_2 and TiO_2 based sensors can detect hydrogen molecules at the low concentration range of 5–10 ppm,[5,6] *i.e.*, about 10^{-7} mol L^{-1}; and Pd nonoparticle decorated ZnO nanorods can detect hydrogen molecules at the even lower concentration of 0.2 ppm,[7] *i.e.*, about 10^{-8} mol L^{-1}. Compared with these results, graphene with mono-atom vacancies has ultra-high sensitivity for H_2 detection at room temperature.

4. Conclusion

In summary, the effects of vacancies on the dissociative adsorption of H_2 molecules on graphene are investigated through DFT calculations. The results show that graphene with a mono-atom-vacancy can efficiently reduce the dissociative energy barrier of H_2 molecules on graphene and two H_2 molecules can be dissociatively adsorbed at each vacancy even when the concentration of H_2 is as low as 10^{-35} mol L^{-1}. Based on the calculated band structures, the electronic properties change significantly after the hydrogen dissociative adsorption. Therefore, graphene with a mono-atom-vacancy has potential for ultra-low concentration hydrogen detection.

Acknowledgements

References

1 M. Balat, *Int. J. Hydrogen Energy*, 2008, **33**, 4013–4029.
2 W. J. Buttner, M. B. Post, R. Burgess and C. Rivkin, *Int. J. Hydrogen Energy*, 2011, **36**, 2462–2470.
3 O. K. Varghese, D. Gong, M. Paulose, K. G. Ong and C. A. Grimes, *Sens. Actuators, B*, 2003, **93**, 338–344.
4 G. K. Mor, O. K. Varghese, M. Paulose, K. G. Ong and C. A. Grimes, *Thin Solid Films*, 2006, **496**, 42–48.
5 B. Wang, L. F. Zhu, Y. H. Yang, N. S. Xu and G. W. Yang, *J. Phys. Chem. C*, 2008, **112**, 6643–6647.
6 C. Lu and Z. Chen, *Sens. Actuators, B*, 2009, **140**, 109–115.
7 T.-R. Rashid, D.-T. Phan and G.-S. Chung, *Sens. Actuators, B*, 2013, **185**, 777–784.
8 T. Waitz, T. Wagner, T. Sauerwald, C.-D. Kohl and M. Tiemann, *Adv. Funct. Mater.*, 2009, **19**, 653–661.
9 K. S. Novoselov, A. K. Geim, S. V. Morozov, D. Jiang, Y. Zhang, S. V. Dubonos, I. V. Grigorieva and A. A. Firsov, *Science*, 2004, **306**, 666–669.
10 K. S. Novoselov, A. K. Geim, S. V. Morozov, D. Jiang, M. I. Katsnelson, I. V. Grigorieva, S. V. Dubonos and A. A. Firsov, *Nature*, 2005, **438**, 197–200.
11 C. G. Lee, X. D. Wei, J. W. Kysar and J. Hone, *Nature*, 2008, **321**, 385–388.
12 Y. Miura, H. Kasai, W. Diño, H. Nakanishi and T. Sugimoto, *J. Appl. Phys.*, 2003, **93**, 3395–3400.
13 F. Banhart, J. Kotakoski and A. V. Krasheninnikov, *ACS Nano*, 2011, **5**, 26–41.
14 D. Li, M. B. Muller, S. Gilje, R. B. Kaner and G. G. Wallace, *Nat. Nanotechnol.*, 2008, **3**, 101–105.
15 L. Tapasztó, G. Dobrik, P. Nemes-Inczel, G. Vertesy, P. Lambin and L. P. Biró, *Phys. Rev. B: Condens. Matter Mater. Phys.*, 2008, **78**, 233407.
16 O. Lehtinen, J. Kotakoski, A. V. Krasheninnikov, A. Tolvanen, K. Nordlund and J. Keinonen, *Phys. Rev. B: Condens. Matter Mater. Phys.*, 2010, **81**, 153401.
17 P. O. Lehtinen, A. S. Foster, Y. C. Ma, A. V. Krasheninnikov and R. M. Nieminen, *Phys. Rev. Lett.*, 2004, **93**, 187202.
18 A. Allouche and Y. Ferro, *Carbon*, 2006, **44**, 3320–3327.
19 B. H. Kim, S. J. Hong, S. J. Baek, H. Y. Jeong, N. Park, M. Lee, S. W. Lee, M. Park, S. W. Chu, H. S. Shin, J. Lim, J. C. Lee, Y. Jun and Y. W. Park, *Sci. Rep.*, 2012, **2**, 690.
20 B. Delley, *J. Chem. Phys.*, 2000, **113**, 7756–7764.
21 J. P. Perdew, K. Burke and M. Ernzerhof, *Phys. Rev. Lett.*, 1996, **77**, 3865.
22 A. Roldán, J. M. Ricart and F. Illas, *Theor. Chem. Acc.*, 2009, **123**, 119–126.
23 T. A. Halgren and W. N. Lipscomb, *Chem. Phys. Lett.*, 1977, **49**, 225–232.
24 G. Henkelman and H. Jonsson, *J. Chem. Phys.*, 2000, **113**, 9978–9985.
25 S. Grimme, *J. Comput. Chem.*, 2006, **27**, 1787–1789.
26 K. Reuter and M. Scheffler, *Phys. Rev. B: Condens. Matter*, 2001, **65**, 035406.
27 Z. X. Yang, Q. G. Wang, S. Y. Wei, D. W. Ma and Q. Sun, *J. Phys. Chem. C*, 2010, **114**, 14891–14899.

This journal is © the Owner Societies 2013

Phys. Chem. Chem. Phys., 2013, **15**, 21016–21022 | **21021**

28 M. D. Segall, P. L. D. Lindan, M. J. Probert, C. J. Pickard, P. J. Hasnip, S. J. Clark and M. C. Payne, *J. Phys.: Condens. Matter*, 2002, **14**, 2717–2744.

29 K. Reuter and M. Scheffler, *Phys. Rev. B: Condens. Matter*, 2001, **65**, 035406.

30 NIST Chemistry Web book: http://webbook.nist.gov/.

31 C. Q. Sun, Y. G. Nie, J. S. Pan, X. Zhang, S. Z. Ma, Y. Wang and W. T. Zheng, *RSC Adv.*, 2012, **2**, 2377–2383.

32 M. Amft, S. Lebègue, O. Eriksson and N. V. Skorodumova, *J. Phys.: Condens. Matter*, 2011, **23**, 395001.

33 E. Ganz, K. Sattler and J. Clarke, *Surf. Sci.*, 1989, **219**, 33–67.

34 F. Costanzo, P. L. Silvestrelli and F. Ancilotto, *J. Chem. Theory Comput.*, 2012, **8**, 1288–1294.

35 D. C. Young, *Computational Chemistry: A Practical Guide for Applying Techniques to Real World Problems*, Wiley, New York, 2001.